



Layer-by-layer assembly of layered double hydroxide/rubber multilayer films with excellent gas barrier property



Lumei Wang^a, Yibo Dou^b, Jiajie Wang^a, Jingbin Han^{a,*}, Li Liu^a, Min Wei^a

^a State Key Laboratory of Chemical Resource Engineering, Beijing University of Chemical Technology, Beijing 100029, PR China

^b Beijing Key Laboratory for Green Catalysis and Separation and Department of Chemistry and Chemical Engineering, Beijing University of Technology, Beijing 100124, PR China

ARTICLE INFO

Article history:

Received 11 May 2017

Received in revised form 23 June 2017

Accepted 12 July 2017

Available online 14 July 2017

Keywords:

Gas barrier

Rubber

Layered double hydroxides

Multilayer film

ABSTRACT

Rubber nanocomposites with high gas barrier property have extensive application prospects in sealing and packing industry, while developing a novel and cost-effective rubber-based material with low gas permeability and good mechanical property still remains a challenge. Herein, we designed and fabricated an excellent gas barrier film by using polyvinyl pyrrolidone modified ultrathin layered double hydroxide nanoplatelets (U-mLDH) and nitrile butadiene rubber (NBR) as building blocks. The resultant (U-mLDH/NBR)₃₀ film displays significantly decreased (reduced by 92.2% compared with NBR film) oxygen transmission rate with 0.626 cm³ m⁻² day⁻¹ atm⁻¹, and much lower relative permeability in comparison with reported rubber composites. The improved gas barrier performance is ascribed to the prolonged passage of oxygen molecules and the decreased free space arising from large aspect ratio of U-mLDH and good interfacial compatibility. In addition, the (U-mLDH/NBR)₃₀ film also possesses high thermal stability and satisfactory mechanical property, which would guarantee its practical applications.

© 2017 Elsevier Ltd. All rights reserved.

1. Introduction

Rubber products hold great promise on a variety of applications, including automobile tire, outdoor sealing and aerospace engineering [1,2]. Nitrile butadiene rubber (NBR) is one of the most extensively used synthetic rubber due to its high water resistance, good adhesive property and excellent thermal/chemical stability [3–6]. However, its relatively high gas permeability restricts the application as inner liner of tire and sealing materials. Carbon black and white carbon black are generally used as rubber additives to improve its gas barrier property. Nevertheless, the mass loading of these additives should be very high to meet the requirement of low gas permeability, which finally results in poor flexibility and inferior mechanical toughness of the composite materials [7,8]. In order to solve this problem, two-dimensional (2D) inorganic platelets would be promising candidates to be incorporated into a polymer matrix to achieve high-performance gas barrier materials [9–15], because their anisotropic morphology would induce an extensive diffusion path for the diffusing gas and hence hinder the gas permeation.

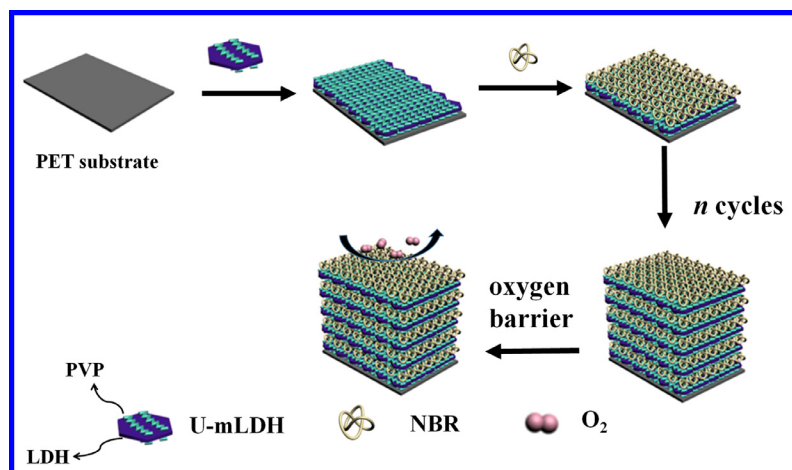
Layered double hydroxides (LDHs) are an unusual family of 2D inorganic layered material consisting of positively charged layers with charge-balancing anions between the brucite-like layers

[16–20], which have been applied to fabricate organic-inorganic hybrid materials with fascinating properties [21–23]. Experimental and simulated investigations have revealed that the aspect ratios of inorganic fillers is of key importance for gas barrier property of the hybrids [10], i.e. higher aspect ratio can induce longer diffusion length for gas permeation and thus a better barrier behavior. Single layered LDH nanosheet with large aspect ratio (>1000) has been achieved by exfoliation of bulk materials [24,25], which is regarded as an ideal building block to construct hybrid gas barrier films. However, the exfoliation process is time-consuming and the yield is rather low. Therefore, the large-scale production of ultrathin LDH nanosheet is the crucial step to achieve practical application of such nanosheets. In addition, the surface hydrophilicity of LDHs generally induces poor dispersion and aggregation into organic matrix, even phase separation [26–29], which deteriorates the gas property of the composites. As a result, the pristine LDHs have to be modified by organics to construct a better interfacial interaction for improving the dispersion of LDHs in organic matrix [30–33].

In this work, we have synthesized ultrathin LDH (U-LDH) nanoplatelets followed by surface modification with polyvinyl pyrrolidone (PVP) (named as U-mLDH), which were alternately assembled with NBR to prepare hybrid films (Scheme 1). The obtained (U-mLDH/NBR)_n film displays much lower relative permeability, in comparison with reported rubber-based composites. The excellent gas barrier performance is attributed to the

* Corresponding author.

E-mail address: hanjb@mail.buct.edu.cn (J. Han).



Scheme 1. Schematic illustration for the assembly of $(U\text{-mLDH}/NBR)_n$ film on PET substrate by layer-by-layer assembly technique.

extremely high aspect ratio of U-mLDH nanoplatelets and good interfacial compatibility, which could largely prolong the diffusion path of gas molecules and decrease the free volume for gas permeation. Simultaneously, the $(U\text{-mLDH}/NBR)_n$ film exhibits good thermal stability and satisfying mechanical property.

2. Experimental section

2.1. Reagents and materials

Nitrile butadiene rubber (NBR) was purchased from Shanghai NESSEN international trading Co. Ltd. Polyvinyl pyrrolidone (PVP)

was obtained from Xilong Chemical Co. Ltd. $Mg(NO_3)_2 \cdot 6H_2O$, $Al(NO_3)_3 \cdot 9H_2O$, NaOH, $NaNO_3$, formamide, ethanol and acetone were analytical grade chemicals and used without further purification.

2.2. Synthesis of ultrathin LDH (U-LDH) and normal LDH (N-LDH)

Two kinds of LDHs with different aspect ratios were prepared, i.e. ultrathin LDH (U-LDH) and normal LDH (N-LDH). The U-LDH was synthesized by a slightly improved co-precipitation strategy based on other's report [34]. Briefly, a solution of $Mg(NO_3)_2 \cdot 6H_2O$ (0.02 M) and $Al(NO_3)_3 \cdot 9H_2O$ (0.01 M) was added dropwise to $NaNO_3$ (0.01 M) solution containing 23 vol% formamide with

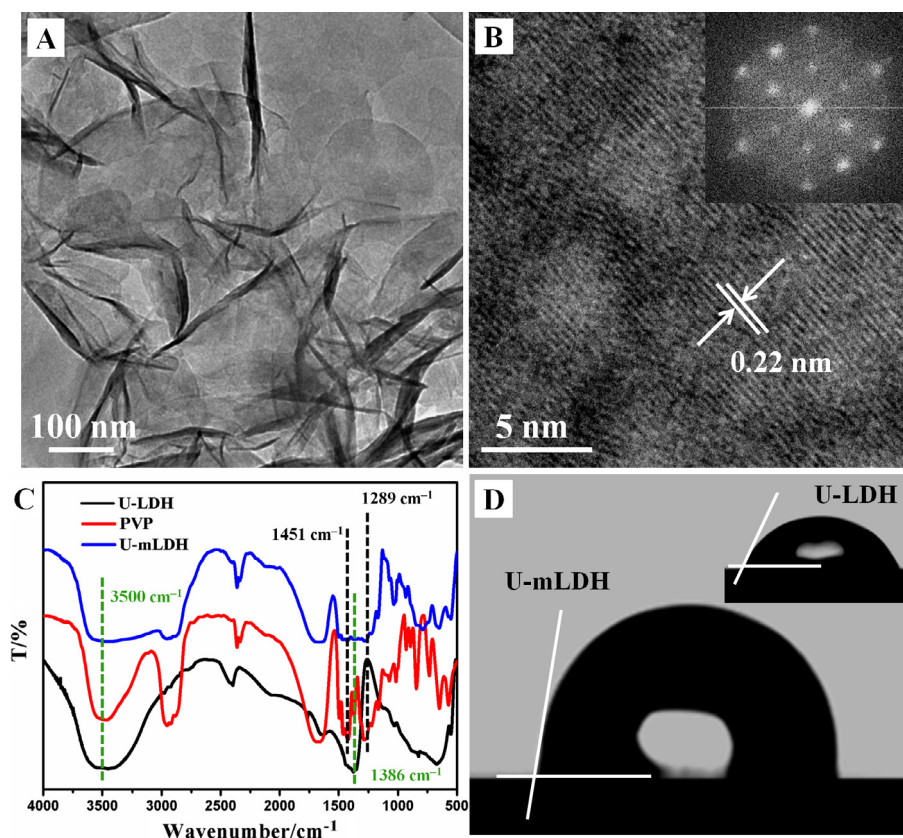


Fig. 1. (A) HR-TEM images of U-LDH; (B) The lattice fringe of U-LDH (inset: the fast Fourier transform image); (C) FT-IR spectra of U-LDH, PVP and U-mLDH powder samples; (D) Water contact angle of the U-mLDH and U-LDH thin films. (For interpretation of the references to colour in this figure legend, the reader is referred to the web version of this article.)

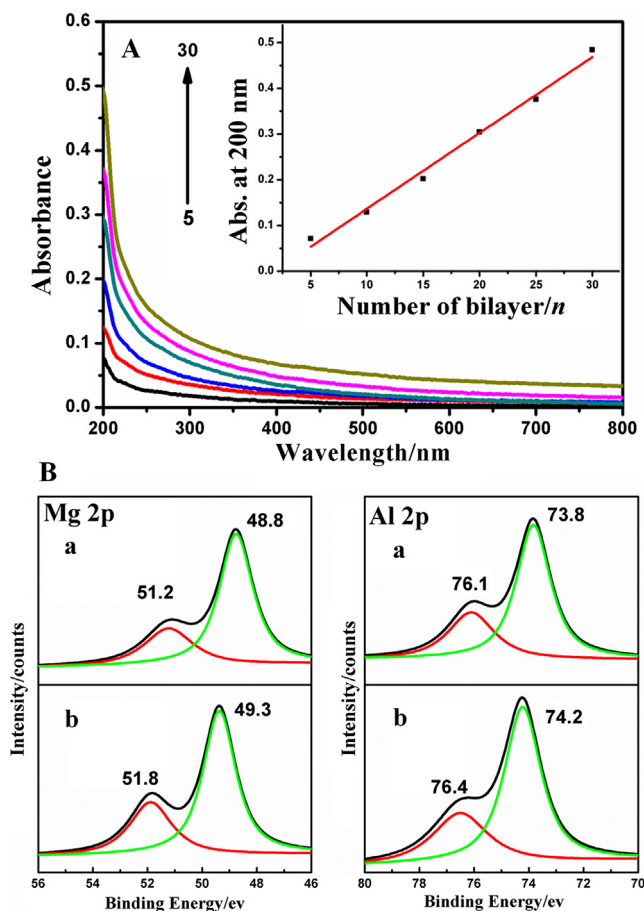


Fig. 2. (A) UV-vis absorption spectra of the (U-mLDH/NBR) $_n$ ($n = 5-30$) films (inset: absorbance at 200 nm plotted against the bilayer number n); (B) Mg 2p, Al 2p XPS spectra of (a) U-mLDH nanoplatelet and (b) (U-mLDH/NBR) $_30$ film. (For interpretation of the references to colour in this figure legend, the reader is referred to the web version of this article.)

0.25 M NaOH solution under the following conditions: magnetic stirring at 80 °C and maintaining pH at ca. 10. After reaction for 1 h, the U-LDH suspension was obtained.

N-LDH (as control sample for comparing study) was obtained by using a method that involves separate nucleation and aging steps (SNAS) [35]. Typically, 100 ml solution composed by Mg(NO₃)₂·6H₂O (0.20 M) and Al(NO₃)₃·9H₂O (0.10 M) were simultaneously added to a colloid mill with 400 ml NaOH (0.15 M) solution under the conditions: rotor speed of 3000 rpm and mixing time of 1 min. The resulting LDH slurry was transferred into a stainless steel autoclave with a Teflon lining. After hydrothermal treatment at 110 °C for 24 h, stable homogeneous LDH suspension was obtained *via* centrifugation, washed with water and then dispersed in 400 ml deionized water.

2.3. Surface modification of U-LDH and N-LDH

Five times mass of PVP was added into the U-LDH aqueous suspension (0.028 wt%) and stirred for 2 h at room temperature. The product was washed several times *via* centrifugation and then dispersed in water to form stable suspension. The modification of N-LDH was similar with this procedure.

2.4. Fabrication of (U-mLDH/NBR) $_n$ multilayer films

The U-mLDH was used as building blocks to fabricate (U-mLDH/NBR) $_n$ films by the layer-by-layer assembly technique. The silicon

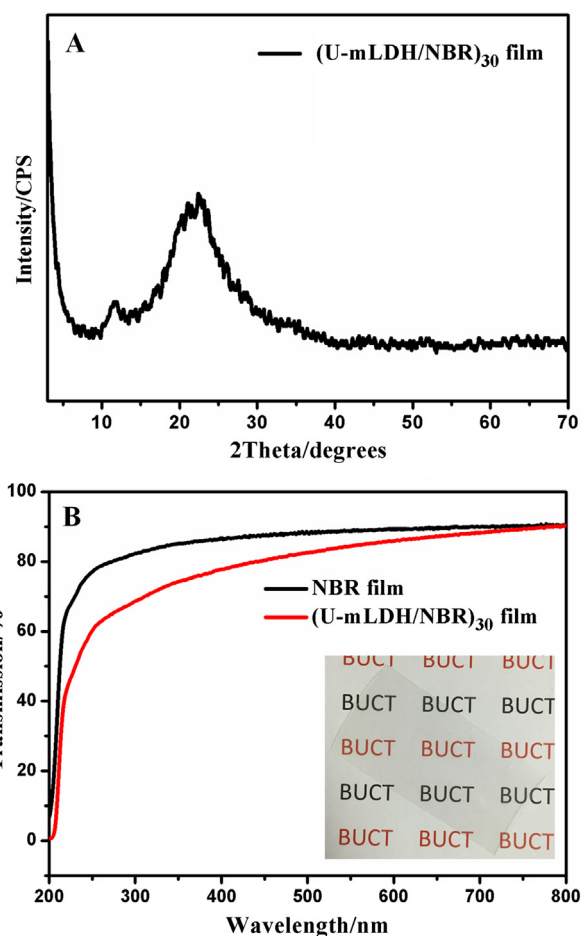


Fig. 3. (A) XRD pattern of the (U-mLDH/NBR) $_30$ film; (B) Light transmission as a function of wavelength for the NBR and the (U-mLDH/NBR) $_30$ films (inset: digital photograph of (U-mLDH/NBR) $_30$ film on PET substrate. (For interpretation of the references to colour in this figure legend, the reader is referred to the web version of this article.)

wafer, quartz glass and poly(ethylene terephthalate) (PET) films were used as substrates for various characterizations. U-mLDH suspension and NBR solution (1 wt%) were spin-coated onto the substrate with 2000 rpm and 4000 rpm for 60 s alternately. By repeating the above operations for n times, (U-mLDH/NBR) $_n$ films were obtained. The control samples, including (U-LDH/NBR) $_n$, (N-mLDH/NBR) $_n$ and pure NBR films, were fabricated by a similar layer-by-layer spin-coating process.

3. Results and discussion

3.1. Characterization of U-LDH, N-LDH and U-mLDH

Powder X-ray diffraction (XRD) pattern (Fig. S1, Supporting Information) of the U-LDH shows a series of reflections at 11.1°, 22.4°, 34.4°, 60.0° and 61.2°, corresponding to characteristic (003), (006), (012), (110) and (113) reflections of the carbonate-containing LDH phase. Fig. 1A shows ultrathin feature of the LDH nanoplatelets with lateral size of 300–800 nm and slab thickness ranging in 1–3 nm. An identified reflection patterns with interplanar distances of 0.22 nm (Fig. 1B) is observed from the typical HR-TEM image of the nanoplatelets, attributed to the (015) plane of LDH phase. The XRD pattern of N-LDH also exhibits a series of reflections at the same location as that of U-LDH, with stronger and more completed diffraction peaks (Fig. S2, Supporting Information), indicating the higher crystallinity of N-LDH. In con-

trast to U-LDH nanoplatelets, the N-LDH displays smaller platelet size and bigger slab thickness (Fig. S3, Supporting Information), illustrating a much lower aspect ratio than U-LDH. A clear Tyndall light scattering over the transparent U-LDH suspension (Fig. S4, Supporting Information) indicates the homogeneity of the colloidal solution.

In order to improve the compatibility of U-LDH with NBR matrix, PVP was modified on the surface of U-LDH nanoplatelets. The FT-IR spectrum (Fig. 1C) illustrates the existence of carbonate ($\sim 1386\text{ cm}^{-1}$) and hydroxyl ($\sim 3500\text{ cm}^{-1}$) of U-LDH (black line); and after modified with PVP, there are new infrared absorption bands at $\sim 1451\text{ cm}^{-1}$ ($\sigma_{\text{C-N}}$) and $\sim 1289\text{ cm}^{-1}$ ($\gamma_{\text{-CH}_2}$) (blue line), indicating successful adsorption of PVP on U-LDH nanoplatelets. In addition, a variation in the water contact angle (CA) of the surface ($\sim 80^\circ$ and $\sim 55^\circ$ for U-mLDH and U-LDH film, respectively) was observed after PVP treatment (Fig. 1D). This significant variation of the CA is attributed to the surface modification of U-LDH by PVP, which could improve interface compatibility with NBR.

3.2. Structural and morphological analyses of (U-mLDH/NBR)_n films

UV-vis absorption spectroscopy was applied to monitor the growth of (U-mLDH/NBR)_n composite films after each five deposition cycles, as shown in Fig. 2A. The nearly linear increment of the absorbance at 200 nm as a function of bilayer number *n* was observed (Fig. 2A, inset), which proves uniform and order deposition of (U-mLDH/NBR)_n multilayer films. X-ray photoelectron spectroscopy (XPS) was applied to verify the presence of interfacial bonding between U-mLDH and NBR (Fig. 2B). The Mg 2p orbital binding energy locates at 48.8 and 51.2 eV for LDH; while after assembly with NBR, the two peaks move to 49.3 and 51.8 eV, respectively. Simultaneously, the Al 2p orbital binding energy (at 73.8 and 76.1 eV) also undergoes a positive shift upon integrating with NBR. Similar phenomenon was found as well in our previous works [36,37]. This result suggests the formation of hydrogen bonds between the hydroxyl groups on the LDH and N atom in the NBR.

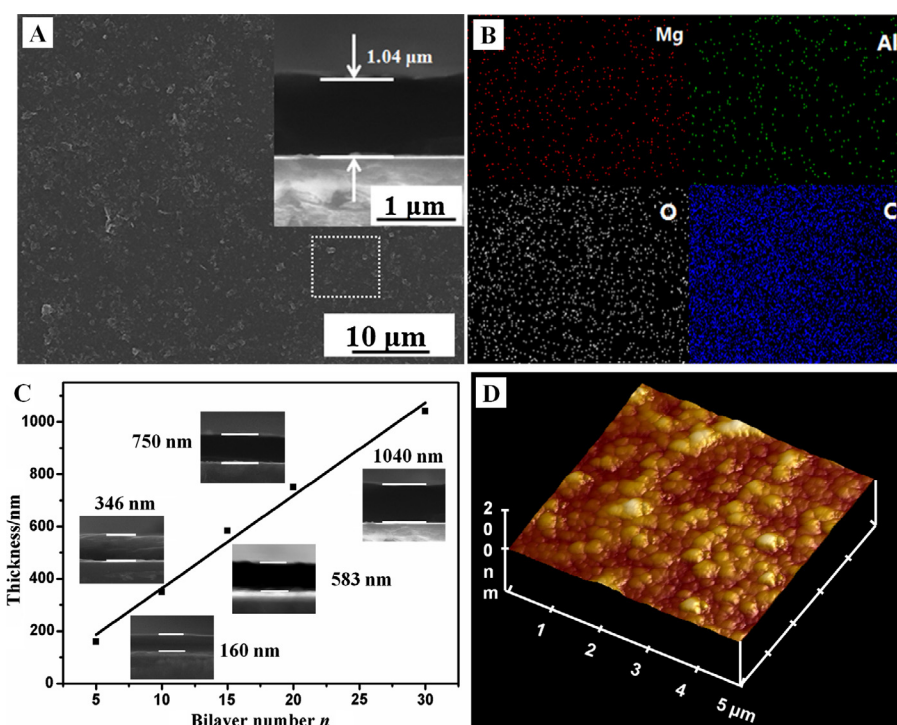


Fig. 4. (A) Top-view SEM image (inset: cross-sectional image); (B) EDX mapping of Mg, Al, O and C for (U-mLDH/NBR)₃₀ film; (C) Thickness of the (U-mLDH/NBR)_n films as a function of bilayer number *n*; (D) AFM height image of the (U-mLDH/NBR)₃₀ film deposited on a polished silicon wafer. (For interpretation of the references to colour in this figure legend, the reader is referred to the web version of this article.)

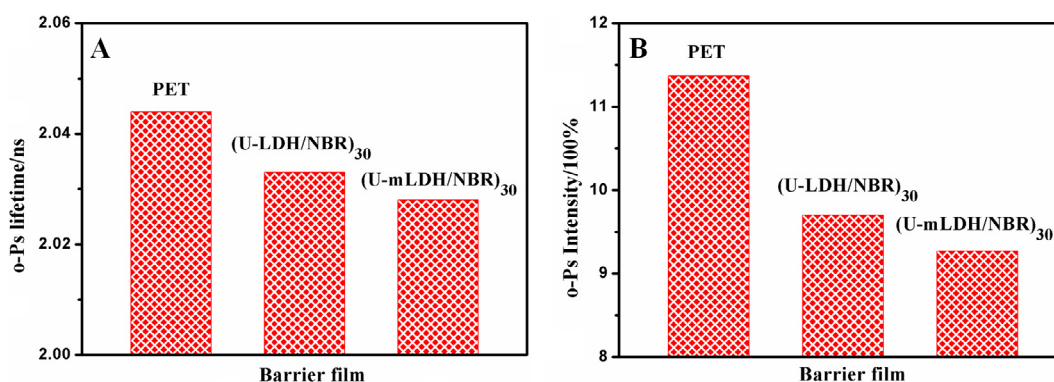


Fig. 5. (A) O-Ps lifetime (τ_3) and (B) relative intensity (I_3) of PET, (U-LDH/NBR)₃₀ and (U-mLDH/NBR)₃₀ film, respectively. (For interpretation of the references to colour in this figure legend, the reader is referred to the web version of this article.)

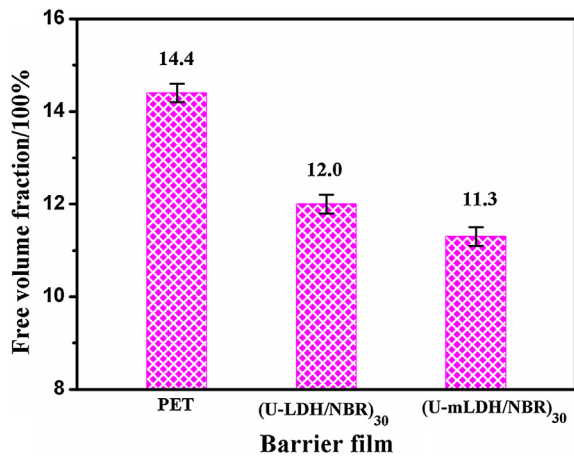


Fig. 6. Free volume fraction of the pristine PET substrate, (U-LDH/NBR)₃₀ film and (U-mLDH/NBR)₃₀ film. (For interpretation of the references to colour in this figure legend, the reader is referred to the web version of this article.)

The XRD pattern of (U-mLDH/NBR)₃₀ film shows a single peak (at 11.54°) ascribed to (003) reflection of LDH without other diffraction peaks, meaning the favorable orientation of U-mLDH nanoplatelets with *ab* plane parallel to the substrate (Fig. 3A). The diffraction at 21.4° can be indexed to the amorphous quartz glass substrate. UV-vis spectroscopy reveals that (U-mLDH/NBR)₃₀ film has an excellent optical transmittance as high as 80% in the wavelength of visible region, as shown in Fig. 3B. This high level of transparency is ascribed to the good dispersion and well orientation of U-mLDH nanoplatelets in the film. The photograph

of the film in Fig. 3B inset shows visually its good optical transparency.

The (U-mLDH/NBR)₃₀ film exhibits a dense and smooth surface with average thickness of 1.04 μm, as evidenced by top-view and cross-sectional SEM images (Fig. 4A). The energy dispersive X-ray spectroscopy (EDX) mapping studies exhibit the uniform dispersion of Mg, Al, O and C elements in Fig. 4B. Moreover, the film thickness increases linearly with the bilayer number *n* (Fig. 4C), further verifying that LDH nanoplatelets and NBR are uniformly deposited by the layer-by-layer spin-coating technique. Surface topography change of the composite films accompanied by the assembled bilayer number was presented by AFM height images (Fig. 4D and Fig. S5, Supporting Information), which show a root-mean-square roughness ranging in 8.1–28.3 nm, further demonstrating a continuous and smooth surface for the (U-mLDH/NBR)_n films.

It has been realized that the free volume is closely related with the gas transmission rates of a barrier film [21,38], which can be examined by using positron annihilation lifetime spectroscopy (PALS) technique based on an infinite potential spherical model. The two parameters, positron lifetime component (τ_3) and relative intensity (I_3) (Fig. 5), can be used to calculate the fraction of free volume (F_v) according to the following two formulas:

$$\tau_3 = \frac{1}{2} \left[1 - \frac{R}{R + 0.166} + \frac{1}{2\pi} \sin \left(\frac{2\pi R}{R + 0.166} \right) \right]^{-1}$$

$$F_v = C \left(\frac{4\pi}{3} R^3 \right) I_3$$

where *R* is the free volume. Compared to the free volume fraction of PET substrate (14.4%), F_v value of the (U-LDH/NBR)₃₀ film drops

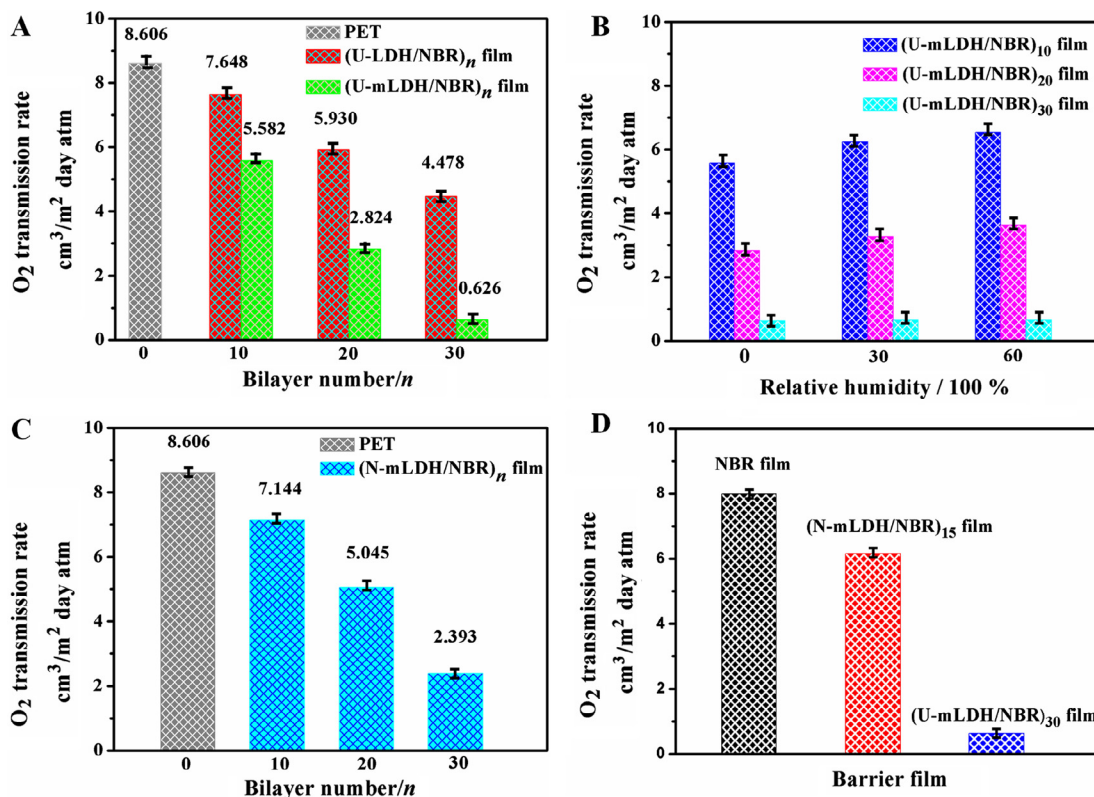


Fig. 7. (A) O₂TR values for pristine PET, (U-LDH/NBR)_n and (U-mLDH/NBR)_n films (*n* = 10, 20 and 30); (B) O₂TR values for (U-mLDH/NBR)_n films as a function of relative humidity (0%, 30% and 60%); (C) O₂TR values of PET substrates coated with (N-mLDH/NBR)_n multilayer films as a function of bilayer number *n*; (D) O₂TR values for pure NBR, (N-mLDH/NBR)₁₅ and (U-mLDH/NBR)₃₀ films with nearly the same thickness (~1 μm), respectively. (For interpretation of the references to colour in this figure legend, the reader is referred to the web version of this article.)

Table 1

Comparison study of gas permeability and relative permeability of the (U-mLDH/NBR)₃₀ film in this work, with previously reported rubber-based nanocomposites.

Film materials	Gas	Gas permeability (cm ³ ·cm/cm ² ·s·Pa)	Relative permeability (P/P ₀)
LDH/XNBR [39]	Air	8.31 * 10 ⁻¹²	–
SGO/NR [40]	Air	2.90 * 10 ⁻¹³	0.45
NR/SMK [41]	N ₂	5.10 * 10 ⁻¹³	0.61
IIR/S-OCN [42]	N ₂	6.32 * 10 ⁻¹⁴	0.78
NR/RGO [43]	O ₂	–	0.32
SR/St-LDH [44]	O ₂	1.19 * 10 ⁻⁸	0.18
Butyl rubber/ vermiculite [45]	O ₂	–	<0.01
This work	O ₂	1.35 * 10 ⁻¹⁶	0.08

down to 12.0%, which reveals that the filling of U-LDH nanoplatelets reduces the free volume fraction of NBR matrix. Further decline of F_v (11.3%) was observed for (U-mLDH/NBR)₃₀ film using modified U-LDH as building blocks, which is ascribed to the improved interfacial compatibility by surface modification of U-LDH nanoplatelets (see Fig. 6).

3.3. The study of oxygen barrier properties for the (U-LDH/NBR)_n, (N-mLDH/NBR)_n and (U-mLDH/NBR)_n films

The barrier properties of (U-LDH/NBR)_n, (N-mLDH/NBR)_n and (U-mLDH/NBR)_n films deposited on a PET substrate were tested at 23 °C and 0% relative humidity, using oxygen transmission rates (O₂TR) measurements. Firstly, we have studied the impact of surface modification of LDH nanoplatelets on gas permeability of various films. Pristine PET substrate shows an O₂TR value of 8.606 cm³ m⁻² day⁻¹ atm⁻¹. The coating of (U-mLDH/NBR)_n films results in an apparent decrease of O₂TR value from 5.582 to 0.626 cm³ m⁻² day⁻¹ atm⁻¹, with increasing the number of bilayers from 10 to 30 (Fig. 7A). The (U-LDH/NBR)_n films manifests the same decreasing O₂TR trend as (U-mLDH/NBR)_n films, but with higher values at the same number of bilayers, which is ascribed to the poor interfacial compatibility between unmodified U-LDH and NBR. In addition, the O₂TR value for (U-mLDH/NBR)₃₀ film measured under various relative humidity displays negligible variation (Fig. 7B), demonstrating its weak dependence against humidity.

The influence of aspect ratio for LDH nanoplatelets on gas transmission was further investigated. The O₂TR values of (N-mLDH/NBR)_n films are 7.144, 5.045 and 2.393 cm³ m⁻² day⁻¹ atm⁻¹ with $n = 10, 20$ and 30 (Fig. 7C), respectively, which are higher than those of (U-mLDH/NBR)_n films with the same bilayer number. This result demonstrates the favorable effect of high aspect ratio of

inorganic component on the enhancement of barrier property for organic-inorganic hybrid films. Moreover, the O₂TR values of various films with the same thickness were compared as well (Fig. 7D). A ~1 μm thick pure NBR film was fabricated by multistep spin-coating technique; and a (N-mLDH/NBR)₁₅ film with the same thickness was obtained by controlling the number of coating cycles. The pure NBR film exhibits an O₂TR of 7.995 cm³ m⁻² day⁻¹ atm⁻¹. While the incorporation of U-mLDH nanoplatelet induces a significantly decrease (reduced by 92.2%) of gas transmission rate to 0.626 cm³ m⁻² day⁻¹ atm⁻¹ for (U-mLDH/NBR)₃₀ film (thickness: ~1.04 μm). In contrast, the ~1 μm thick (N-mLDH/NBR)₁₅ film shows an inferior gas barrier property (O₂TR = 6.106 cm³ m⁻² day⁻¹ atm⁻¹) to the (U-mLDH/NBR)₃₀ film.

The gas barrier property of (U-mLDH/NBR)₃₀ film was further compared with other previously reported rubber composites in the literatures (Table 1). It is clearly seen from the table that the (U-mLDH/NBR)₃₀ film has a better barrier behavior: much lower gas permeability and relative permeability (P/P_0) than the reported rubber-based barrier materials. The excellent barrier performance of (U-mLDH/NBR)₃₀ film is ascribed to the high aspect ratio of U-mLDH platelets and improved interfacial compatibility, which induce a prolonged gas diffusion path and decreased free volume, thus resulting in low gas permeability of the composite films.

3.4. The thermal stability and mechanical property of (U-mLDH/NBR)_n films

Considering the practical applications of the (U-mLDH/NBR)_n films, the thermal stability and mechanical property were also investigated. Thermogravimetric analysis shows the weight of (U-mLDH/NBR)₃₀ film on PET substrate does not undergo apparent change before the temperature increases to 350 °C (Fig. 8A). The onset temperature of (U-mLDH/NBR)₃₀ film is higher than that of reported gas barrier materials (onset temperature = 230–330 °C) [46–49]. Additionally, the (U-mLDH/NBR)₃₀ film exhibits a yielding stress of ~89 MPa with elongation at break of ~92%. In contrast, the pure NBR film shows a lower yielding stress (~78 MPa) and higher elongation at break (~110%) (Fig. 8B). These results illustrate the high thermal stability and good mechanical properties of (U-mLDH/NBR)_n film. Therefore, the low O₂TR value, satisfactory thermal stability and mechanical property would impart the composite (U-mLDH/NBR)_n films a huge application prospect.

4. Conclusions

In this work, we report the fabrication of (U-mLDH/NBR)_n multilayer films with enhanced gas barrier property via layer-by-layer

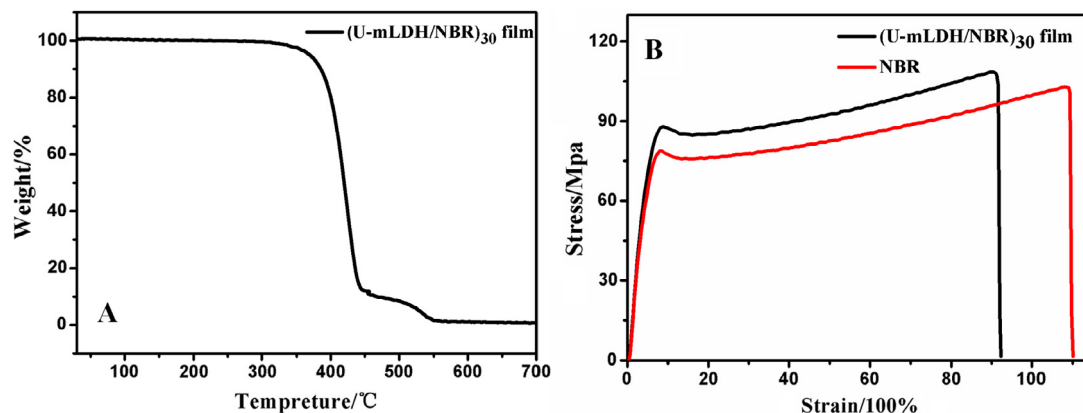


Fig. 8. (A) Thermogravimetric curve and (B) the stress–strain curves for (U-mLDH/NBR)₃₀ film and pure NBR film. (For interpretation of the references to colour in this figure legend, the reader is referred to the web version of this article.)

spin-coating U-mLDH nanoplatelets and NBR. The U-mLDH with large aspect ratio prevents the gas penetration in the composite films by prolonging the passage for oxygen molecules. Moreover, interfacial compatibility is enhanced by surface modification of U-LDH, resulting in low free volume for gas diffusion. This synergistic effect leads to an excellent gas barrier property for the (U-mLDH/NBR)_n films, which is among the highest level in comparison with reported rubber-based composite films. It is prospected that this facile and promising strategy can be used to fabricate high gas barrier material for various applications in vehicle tire and device-sealing industry.

Acknowledgements

This work was supported by the 973 Program (Grant No. 2014CB932102), the National Natural Science Foundation of China (NSFC) and the Beijing Nova Program.

Appendix A. Supplementary material

Supplementary data associated with this article can be found, in the online version, at <http://dx.doi.org/10.1016/j.compositesa.2017.07.014>.

References

- [1] Das A, Wang D, Leuteritz A, Subramaniam K, Greenwell HC, Wagenknecht U, et al. Preparation of zinc oxide free, transparent rubber nanocomposites using a layered double hydroxide filler. *J Mater Chem* 2011;21:7194–200.
- [2] Malas A, Pal P, Giri S, Mandal A, Das CK. Synthesis and characterizations of modified expanded graphite/emulsion styrene butadiene rubber nanocomposites: mechanical, dynamic mechanical and morphological properties. *Compos B-Eng* 2014;58:267–74.
- [3] Zhao Y, Chen ZK, Liu Y, Xiao HM, Feng QP, Fu SY. Simultaneously enhanced cryogenic tensile strength and fracture toughness of epoxy resins by carboxylic nitrile-butadiene nano-rubber. *Compos Part A* 2013;55:178–87.
- [4] Choudhury A, Bhowmick AK, Ong C. Effect of different nanoparticles on thermal, mechanical and dynamic mechanical properties of hydrogenated nitrile butadiene rubber nanocomposites. *J Appl Polym Sci* 2010;116:1428–41.
- [5] Praveen S, Chattopadhyay PK, Albert P, Dalvi VG, Chakraborty BC, Chattopadhyay S. Synergistic effect of carbon black and nanoclay fillers in styrene butadiene rubber matrix: development of dual structure. *Compos Part A* 2009;40:309–16.
- [6] Mao ND, Thanh TD, Thuong NT, Grillet AC, Kim NH, Lee JH. Enhanced mechanical and thermal properties of recycled ABS/nitrile rubber/nanofil N15 nanocomposites. *Compos B-Eng* 2016;93:280–8.
- [7] Surya I, Ismail H. The effect of the addition of alkanolamide on properties of carbon black-filled natural rubber (SMR-L) compounds cured using various curing systems. *Polym Test* 2016;50:276–82.
- [8] Sawai J, Higuchi K, Minami T, Kikuchi M. Permeation characteristics of 4-substituted phenols and anilines in aqueous solution during removal by a silicone rubber membrane. *Chem Eng J* 2009;152:133–8.
- [9] Zhao LL, Yuan BB, Geng YR, Yu CN, Kim NH, Lee JH, et al. Fabrication of ultrahigh hydrogen barrier polyethyleneimine/graphene oxide films by LBL assembly fine-tuned with electric field application. *Compos Part A* 2015;78:60–9.
- [10] Dou Y, Xu S, Liu X, Han J, Yan H, Wei M, et al. Transparent, flexible films based on layered double hydroxide/cellulose acetate with excellent oxygen barrier property. *Adv Funct Mater* 2014;24:514–21.
- [11] Das P, Malho JM, Rahimi K, Schacher FH, Wang B, Demco DE, et al. Nacre-mimetics with synthetic nanoclays up to ultrahigh aspect ratios. *Nat Commun* 2015;6:5967–80.
- [12] Yang Y, Bolling L, Priolo MA, Grunlan JC. Super gas barrier and selectivity of graphene oxide-polymer multilayer thin films. *Adv Mater* 2013;25:503–8.
- [13] Ren PG, Wang H, Yan DX, Huang HD, Wang HB, Zhang ZP, et al. Ultrahigh gas barrier poly (vinyl alcohol) nanocomposite film filled with congregated and oriented Fe₃O₄@GO sheets induced by magnetic-field. *Compos Part A* 2017;97:1–9.
- [14] Follain N, Alexandre B, Chappey C, Colasse L, Mederic P, Marais S. Barrier properties of polyamide 12/montmorillonite nanocomposites: effect of clay structure and mixing conditions. *Compos Sci Technol* 2016;136:18–28.
- [15] Dou Y, Pan T, Xu S, Yan H, Han J, Wei M, et al. Transparent, ultrahigh-gas-barrier films with a brick-mortar-sand structure. *Angew Chem Int Ed* 2015;54:9673–8.
- [16] Ma R, Takada K, Fukuda K, Iyi N, Bando Y, Sasaki T. Topochemical synthesis of monometallic (Co²⁺-Co³⁺) layered double hydroxide and its exfoliation into positively charged Co(OH)₂ nanosheets. *Angew Chem Int Ed* 2008;47:86–9.
- [17] Wang Q, O'Hare D. Recent advances in the synthesis and application of layered double hydroxide (LDH) nanosheets. *Chem Rev* 2012;112:4124–55.
- [18] Iftikhar S, Srivastava V, Sillanpää M. Synthesis and application of LDH intercalated cellulose nanocomposite for separation of rare earth elements (REEs). *Chem Eng J* 2017;309:130–9.
- [19] Tseng C, Hsueh H, Chen C. Effect of reactive layered double hydroxides on the thermal and mechanical properties of LDHs/epoxy nanocomposites. *Compos Sci Technol* 2007;67:2350–62.
- [20] Zhao MQ, Zhang Q, Huang JQ, Wei F. Hierarchical nanocomposites derived from nanocarbons and layered double hydroxides-properties, synthesis, and applications. *Adv Funct Mater* 2012;22:675–94.
- [21] Pan T, Xu S, Dou Y, Liu X, Li Z, Han J, et al. Remarkable oxygen barrier films based on a layered double hydroxide/chitosan hierarchical structure. *J Mater Chem A* 2015;3:12350–6.
- [22] Raffee F, Otadi M, Goodarzi V, Khonakdar HA, Jafari SH, Mardani E, et al. Thermal and dynamic mechanical properties of PP/EVA nanocomposites containing organo-modified layered double hydroxides. *Compos B-Eng* 2016;103:122–30.
- [23] Xu W, Zhang B, Xu, Li A. The flame retardancy and smoke suppression effect of heptaheptamolybdate modified reduced graphene oxide/layered double hydroxide hybrids on polyurethane elastomer. *Compos Part A* 2016;91:30–40.
- [24] Eshwaran SB, Basu D, Vaikuntam SR, Kutlu B, Wiessner S, Das A, et al. Exploring the role of stearic acid in modified zinc aluminum layered double hydroxides and their acrylonitrile butadiene rubber nanocomposites. *J Appl Polym Sci* 2015;132:41539–47.
- [25] Guo B, Zhao Y, Huang Q, Jiao Q. A new method to prepare exfoliated UV-cured polymer/LDH nanocomposites via nanoplatelet-like LDHs modified with N-Lauroyl-glutamate. *Compos Sci Technol* 2013;81:37–41.
- [26] Liu Z, Ma R, Osada M, Iyi N, Ebina Y, Takada K, et al. Synthesis, anion exchange, and delamination of Co-Al layered double hydroxide: assembly of the exfoliated nanosheet/polyanion composite films and magneto-optical studies. *J Am Chem Soc* 2006;128:4872–80.
- [27] Liang R, Yan D, Tian R, Yu X, Shi W, Li C, et al. Quantum dots-based flexible films and their application as the phosphor in white light-emitting diodes. *Chem Mater* 2014;26:2595–600.
- [28] Compton OC, Kim S, Pierre C, Torkelson JM, Nguyen ST. Crumpled graphene nanosheets as highly effective barrier property enhancers. *Adv Mater* 2010;22:4759–63.
- [29] Ammala A, Pas SJ, Lawrence KA, Stark R, Webb RI, Hill AJ. Poly (m-xylene adipamide)-montmorillonite nanocomposites: effect of organo-modifier structure on free volume and oxygen barrier properties. *J Mater Chem* 2008;18:911–6.
- [30] Utracki LA, Seppehr M, Boccacali E. Synthetic, layered nanoparticles for polymeric nanocomposites (PNCs). *Polym Adv Technol* 2007;18:1–37.
- [31] Stankovich S, Dikin DA, Dommett GHB, Kohlhaas KM, Zimney EJ, Stach EA, et al. Graphene-based composite materials. *Nature* 2006;442:282–6.
- [32] Kwak S, Jun J, Jung ES. Gas barrier film with a compositional gradient interface prepared by plasma modification of an organic/inorganic hybrid sol-gel coat. *Langmuir* 2009;25:8051–5.
- [33] Leroux F, Illaik A, Stimpfling T, Troutier-Thuilliez A, Fleutot S, Martinez H, et al. Percolation network of organo-modified layered double hydroxide platelets into polystyrene showing enhanced rheological and dielectric behavior. *J Mater Chem* 2010;20:9484–94.
- [34] Yu J, Martin BR, Clearfield A, Luo Z, Sun L. One-step direct synthesis of layered double hydroxide single layer nanosheets. *Nanoscale* 2012;7:9448–51.
- [35] Han J, Dou Y, Wei M, Evans DG, Duan X. Erasable nanoporous antireflection coatings based on the reconstruction effect of layered double hydroxides. *Angew Chem Int Ed* 2010;49:2171–4.
- [36] Han J, Dou Y, Yan D, Ma J, Wei M, Evans DG, et al. Biomimetic design and assembly of organic-inorganic composite films with simultaneously enhanced strength and toughness. *Chem Commun* 2011;47:5274–6.
- [37] Dou Y, Han J, Wang T, Wei M, Evans DG, Duan X. Temperature-controlled electrochemical switch based on layered double hydroxide/poly(N-isopropylacrylamide) ultrathin films fabricated via layer-by-layer assembly. *Langmuir* 2012;28:9535–42.
- [38] Eldrup M, Lightbody D, Sherwood JN. The temperature dependence of positron lifetimes in solid pivalic acid. *Chem Phys* 1981;63:51–8.
- [39] Laskowska A, Zaborski M, Boiteux G, Gain O, Marzec A, Maniukiewicz W. Effects of unmodified layered double hydroxides MgAl-LDHs with various structures on the properties of filled carboxylated acrylonitrile-butadiene rubber XNBR. *Eur Polym J* 2014;60:172–85.
- [40] Wu J, Huang G, Li H, Wu S, Liu Y, Zheng J. Enhanced mechanical and gas barrier properties of rubber nanocomposites with surface functionalized graphene oxide at low content. *Polymer* 2013;54:1930–7.
- [41] Zhang Y, Liu Q, Zhang Q, Lu Y. Gas barrier properties of natural rubber/kaolin composites prepared by melt blending. *Appl Clay Sci* 2010;50:255–9.
- [42] Liang Y, Cao W, Li Z, Wang Y, Wu Y, Zhang L. A new strategy to improve the gas barrier property of isobutylene-isoprene rubber/clay nanocomposites. *Polym Test* 2008;27:270–6.
- [43] Scherillo G, Lavorgna M, Buonocore GG, Zhan YH, Xia HS, Mensitieri G, et al. Tailoring assembly of reduced graphene oxide nanosheets to control gas barrier properties of natural rubber nanocomposites. *ACS Appl Mater Interfaces* 2014;6:2230–4.
- [44] Pradhan B, Srivastava SK, Bhowmick AK, Saxenac A. Effect of bilayered stearate ion-modified MgAl layered double hydroxide on the thermal and mechanical properties of silicone rubber nanocomposites. *Polym Int* 2012;61:458–65.

- [45] Takahashi S, Goldberg HA, Feeney CA, Karim DP, Farrell M, O'Leary K, et al. Gas barrier properties of butyl rubber/vermiculite nanocomposite coatings. *Polymer* 2006;47:3083–93.
- [46] Siracusa V, Blanco I, Romani S, Tylewicz U, Rocculi P, Rosa MD. Poly(lactic acid)-modified films for food packaging application: physical, mechanical, and barrier behavior. *J Appl Polym Sci* 2012;125:E390–401.
- [47] Yuwawech K, Wootthikanokkhan J, Tanpichai S. Enhancement of thermal, mechanical and barrier properties of EVA solar cell encapsulating films by reinforcing with esterified cellulose nanofibres. *Polym Test* 2015;48:12–22.
- [48] Bian Q, Tian H, Wang Y, Liu Q, Ge X, Rajulu AV, et al. Effect of graphene oxide on the structure and properties of poly(vinyl alcohol) composite films. *Polym Sci Series A* 2015;57:836–44.
- [49] Kaushik A, Kumra J. Morphology, thermal and barrier properties of green nanocomposites based on TPS and cellulose nanocrystals. *J Elastomers Plast* 2014;46:284–99.